Geophysical Research Letters

RESEARCH LETTER
10.1029/2019GL085335

Key Points:
- Near-terminus sampling at a tidewater glacier reveals ubiquitous meltwater intrusions that are distinct from the subglacial discharge plume
- Meltwater intrusions are only observed within 400 m of the terminus, as they are ultimately entrained into the subglacial discharge plume
- Ambient melt is 2 orders of magnitude higher than standard theory predicts, suggesting a key role for ambient melt in the net ablation

Supporting Information:
- Supporting Information S1

Correspondence to:
R. H. Jackson,
rjackson@marine.rutgers.edu

Citation:
Jackson, R. H., Nash, J. D., Kienholz, C., Sutherland, D. A., Amundson, J. M., Motyka, R. J., et al. (2020). Meltwater intrusions reveal mechanisms for rapid submarine melt at a tidewater glacier. *Geophysical Research Letters*, *47*, e2019GL085335. https://doi.org/10.1029/2019GL085335

Received 10 SEP 2019
Accepted 19 NOV 2019
Accepted article online 25 NOV 2019

©2019. The Authors.
This is an open access article under the terms of the Creative Commons Attribution License, which permits use, distribution and reproduction in any medium, provided the original work is properly cited.

Meltwater Intrusions Reveal Mechanisms for Rapid Submarine Melt at a Tidewater Glacier

R. H. Jackson[1,2], J. D. Nash[2], C. Kienholz[3], D. A. Sutherland[4], J. M. Amundson[3], R. J. Motyka[5], D. Winters[2], E. Skyllingstad[2], and E. C. Pettit[2]

[1]Department of Marine and Coastal Sciences, Rutgers University, New Brunswick, NJ, USA, [2]College of Earth, Ocean, and Atmospheric Sciences, Oregon State University, Corvallis, OR, USA, [3]Department of Natural Sciences, University of Alaska Southeast, Juneau, AK, USA, [4]Department of Earth Sciences, University of Oregon, Eugene, OR, USA, [5]Geophysical Institute, University of Alaska Fairbanks, Fairbanks, AK, USA

Abstract Submarine melting has been implicated as a driver of glacier retreat and sea level rise, but to date melting has been difficult to observe and quantify. As a result, melt rates have been estimated from parameterizations that are largely unconstrained by observations, particularly at the near-vertical termini of tidewater glaciers. With standard coefficients, these melt parameterizations predict that ambient melting (the melt away from subglacial discharge outlets) is negligible compared to discharge-driven melting for typical tidewater glaciers. Here, we present new data from LeConte Glacier, Alaska, that challenges this paradigm. Using autonomous kayaks, we observe ambient meltwater intrusions that are ubiquitous within 400 m of the terminus, and we provide the first characterization of their properties, structure, and distribution. Our results suggest that ambient melt rates are substantially higher (×100) than standard theory predicts and that ambient melting is a significant part of the total submarine melt flux. We explore modifications to the prevalent melt parameterization to provide a path forward for improved modeling of ocean-glacier interactions.

Plain Language Summary Tidewater glaciers discharge ice into the ocean through iceberg calving and submarine melting. Submarine melting has been implicated as a driver of glacier retreat and sea level rise, but melt rates have been difficult to directly observe and quantify. As a result, melt rates are typically estimated using a theory that has not been tested with observations at any tidewater glaciers. Two types of melting are expected at tidewater glaciers: Where subglacial discharge drains from outlets in the terminus, energetic upwelling plumes rise along the ice face, and theory predicts vigorous melting. Away from discharge outlets, weaker plumes form from ambient melting, and theory predicts that these ambient melt rates are effectively negligible compared to discharge-driven melting. Here, we present new data from LeConte Glacier, Alaska, that challenges this paradigm. Using autonomous kayaks, we observe intrusions of meltwater—the product of ambient melt plumes—that are only found within 400 m of the terminus, and we provide the first characterization of their properties, structure, and distribution. Their ubiquity suggests that ambient melt rates are substantially higher than standard theory predicts and that ambient melting is a significant—but often neglected—part of the total submarine melt flux.

1. Background

Mass loss from marine-terminating glaciers is increasing the freshwater flux into the ocean and contributing to rising sea levels (Bamber et al., 2018; Dieng et al., 2017; Shepherd et al., 2018). Glacier dynamics, in turn, are modulated by perturbations at their marine termini from submarine melting and iceberg calving (Ma & Bassis, 2019; Nick et al., 2009). By altering the near-glacier waters that influence submarine melting, ocean variability is thought to have triggered the recent acceleration and retreat of many glaciers (e.g., Alley et al., 2015; Holland et al., 2008; Luckman et al., 2015; Straneo & Heimbach, 2013). However, models of ocean-glacier interaction rely on parameterizations of submarine melting that have not been validated with observations from the near-vertical, calving termini of tidewater glaciers (Straneo & Cenedese, 2015).

In the most common melt parameterizations, heat and salt transfer across the turbulent boundary layer is calculated as a function of near-ice velocity, temperature, and salinity (Holland & Jenkins, 1999; McPhee et al., 1987). At tidewater glaciers, two distinct sources of buoyancy drive velocities near the ice boundary:

(1) Subglacial discharge, fed by surface runoff and precipitation, emerges at the base of termini as a source of localized buoyancy that drives vigorous upwelling (e.g., Slater et al., 2015), and (2) away from these discharge outlets, submarine melting provides a source of distributed buoyancy that drives weak plumes with relatively small upwelling velocities (e.g., Magorrian & Wells, 2016).

At tidewater termini, the near-ice velocity has rarely been measured and is impossible to resolve in most models (due to the small-scale, nonhydrostatic dynamics of plumes), so a common approach for deriving these velocities and associated melt rates is to couple buoyant plume theory (which describes the evolution of a turbulent plume; Ellison & Turner, 1959; Morton et al., 1956) with a submarine melt parameterization (Holland & Jenkins, 1999) to create a coupled plume-melt parameterization (Jenkins, 2011; MacAyeal, 1985). Using this plume-melt framework, the large upwelling velocities from subglacial discharge plumes are expected to drive high melt rates, while the weak velocities of ambient melt plumes produce low melt rates. As a result, for typical tidewater glaciers in Greenland or Alaska, the total ambient melt is often believed to be negligible compared to discharge-driven melt, even after accounting for the substantial difference in surface area between localized discharge plumes and distributed ambient melt (Carroll et al., 2016; Cowton et al., 2015).

Recent studies have thus focused on subglacial discharge plumes, including near-glacier measurements and their comparison with models (Bendtsen et al., 2015; Everett et al., 2018; Jackson et al., 2017; Mankoff et al., 2016). The properties of an energetic subglacial discharge plume are relatively insensitive to melting, because the meltwater flux is dwarfed by the subglacial discharge flux (Slater et al., 2016). Consequently, recent observations of subglacial discharge plumes have been able to test the buoyant plume model within coupled plume-melt theory (Jackson et al., 2017; Mankoff et al., 2016), but these observations provide limited insight into the validity of the melt parameterizations. Ambient melt plumes, on the other hand, should have properties that are sensitive to melting—because meltwater is their only source of buoyancy—and thus they should provide a more direct signal of melt dynamics. However, until now, observations of ambient melt have been lacking.

In the absence of observations, laboratory experiments and theoretical studies have provided a basic foundation for the dynamics of ambient melt plumes and intrusions (Jenkins, 2011; Huppert & Turner, 1980; Magorrian & Wells, 2016): Ambient melting produces a distributed source of buoyancy that forms weak upwelling plumes; as the plumes entrain ocean waters, they lose their buoyancy and form middepth intrusions, where the melt rate and vertical rise of the plumes should scale with the ocean stratification and temperature.

A small but growing body of evidence suggests that we should reconsider ambient melt dynamics. In the standard plume-melt theory, there is a critical assumption that the relevant velocity for melt calculations is the upwelling velocity in buoyant plumes. This results in a self-contained model where melt rates can be predicted based solely on the near-glacier stratification and the influx of subglacial discharge (or lack thereof). However, Slater et al. (2018) suggest that a recirculation gyre—set up by the subglacial discharge plume—should drive horizontal velocities over large swaths of the terminus and thus enhance ambient melt rates. Other studies have also noted that ambient melt rates from the standard plume-melt parameterization seem unrealistically low relative to the total ice flux into the terminus region (Carroll et al., 2016; Fried et al., 2015; Wagner et al., 2019). Finally, melt rates derived from repeat multibeam surveying of LeConte Glacier reveal high melt rates of 1–5 m/day over the entire terminus (Sutherland et al., 2019), suggesting a discrepancy between observed and predicted melt rates but leaving open the question of what melt processes produce these high melt fluxes.

Here, we present the first comprehensive near-glacier observations to characterize ambient melt processes at a tidewater glacier. We find meltwater intrusions to be ubiquitous near the terminus and carry a large quantity of meltwater, indicating that ambient melting is a significant component of the total terminus ablation.

2. Autonomous Near-Terminus Surveying at LeConte Glacier, Alaska

LeConte Glacier is a fast-flowing tidewater glacier (with velocities up to 18 m/day) in southeast Alaska that drains into a proglacial fjord known as LeConte Bay. At the terminus, the glacier is 1 km wide and ~200 m deep. One or two localized subglacial discharge plumes are typically observed at the terminus, resulting in

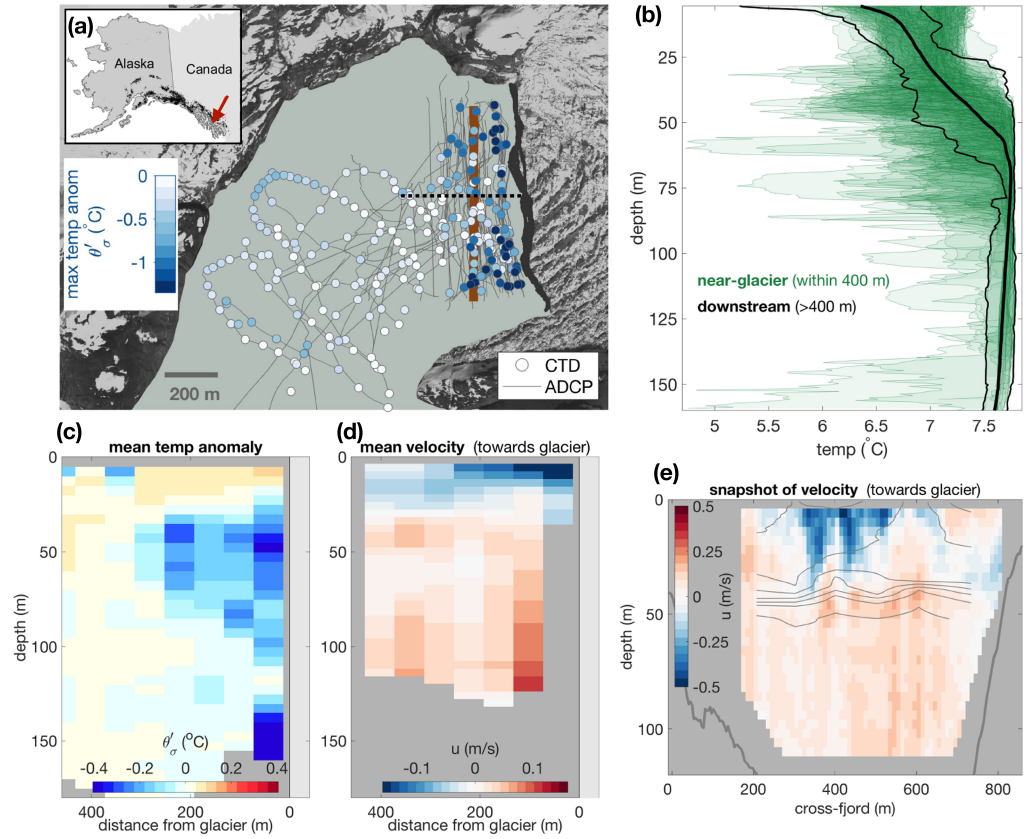

Figure 1. Cold intrusions are ubiquitous in near-glacier region. (a) Satellite image of LeConte Glacier and Bay, with locations of acoustic doppler current profiler sections (ADCP, gray lines) and deep conductivity-temperature-depth casts (CTD, colored circles) collected from kayaks and a ship. Color indicates the maximum isopycnal temperature anomaly (θ'_σ) below 40 m depth for each CTD cast. Terminus positions during the surveying period are shown in black lines. Dashed black line shows transect location for (c) and (d), and thick brown line shows transect location for (e). (b) Temperature of all near-glacier casts within 400 m of the terminus in green lines. Thick black line is the mean downstream temperature (from profiles >400 m from terminus), and thin black lines indicate the envelope that contains all downstream profiles (187 casts). Semitransparent green shading represents the deviation of each near-glacier cast from the downstream mean, such that darker shading indicates a higher concentration of profiles. (c) Mean isopycnal temperature anomaly, from all CTD casts binned as a function of distance from the glacier. (d) Mean eastward velocity (toward the glacier), also bin averaged with distance from the glacier. (e) Snapshot of eastward velocity on 17 September from cross-fjord transect (brown line in (a)) with isopyncals in gray lines spaced every 0.1 kg/m^3.

a near-surface outflow (Motyka et al., 2003) and a recirculation gyre in the fjord's inner basin (Kienholz et al., 2019).

The near-terminus region was surveyed extensively with autonomous kayaks (Nash et al., 2017) over a 7-day period in September 2018 (Figure 1a). Within 350 m of the terminus, the kayaks collected 37 cross-fjord transects of velocity and 166 profiles of temperature and salinity. These near-glacier observations were complemented by downstream shipboard measurements of velocity, temperature, and salinity, with 10 cross-fjord transects occupied between 0.5 and 2 km from the glacier over the same surveying period. (See supporting information for sampling details.)

3. Observations of Meltwater Intrusions From Ambient Melting

The observed velocity patterns are consistent with subglacial discharge-driven circulation (Figures 1d and 1e; Motyka et al., 2003, 2013): A localized discharge plume at the glacier drives an overturning circulation with outflow in the upper 30 m and compensating inflow toward the glacier at depth. However, the most striking feature of the near-glacier profiles is not the subglacial discharge plume but the anomalous properties observed along the rest of the terminus. Within 400 m of the glacier, we observe layers of cold water

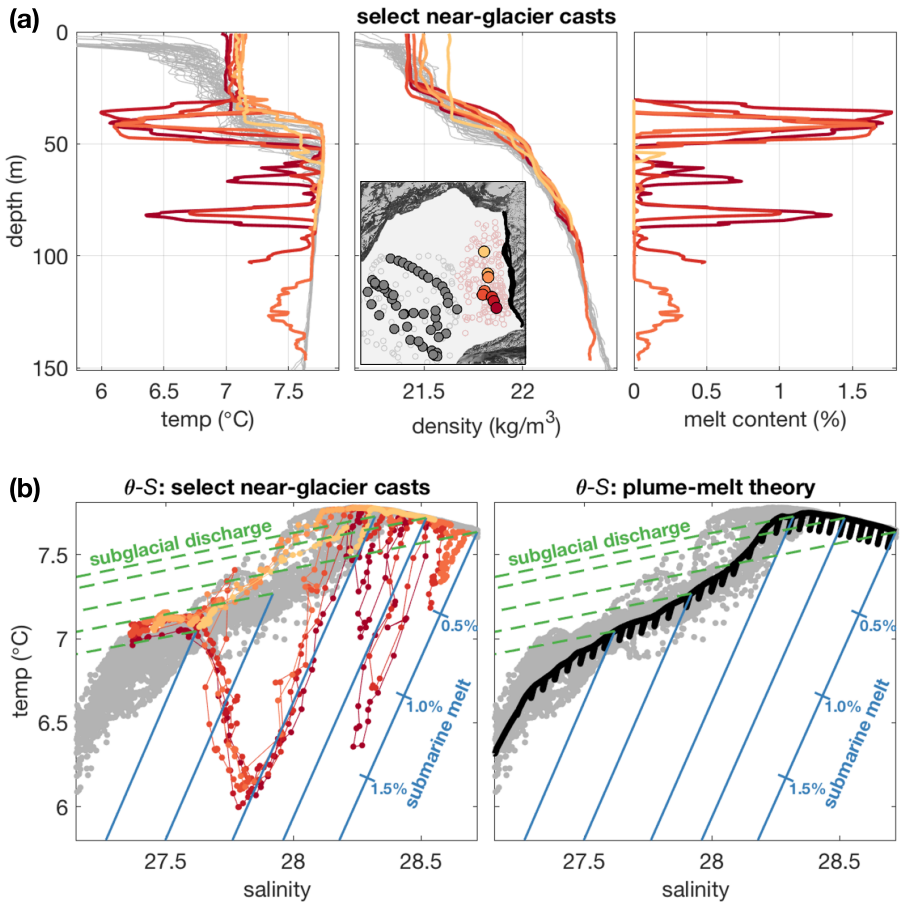

Figure 2. Cold layers are intrusions from ambient melting. Meltwater intrusions in a sample set of CTD casts from a 1.5 hr surveying period on 18 September. Downstream profiles are shown in gray, while near-glacier profiles are shown in shades of red-orange, with locations in inset map. (a) Temperature, density, and meltwater content versus depth. (b) Temperature versus salinity, with mixing lines for submarine melt (blue) and subglacial discharge (dashed green). (left) Same set of casts as (a). (right) Black line shows predicted signal of meltwater intrusions using standard plume-melt theory (supporting information).

that are ~10 m thick and have temperature anomalies of up to −2.2 °C (Figure 1b). These cold layers are ubiquitous near the glacier (63% of casts within 350 m of the terminus have anomalies of at least −0.5 °C) and are most commonly observed in and below the pycnocline at 30 to 70 m depth (Figure 1c).

Submarine melting and subglacial discharge—the two sources of buoyancy at the terminus—leave distinct imprints on temperature-salinity (θ-S) properties because submarine melting requires latent heat from the ocean to melt ice, whereas subglacial discharge is already in liquid form (Gade, 1979). The cold layers have temperature and salinity properties that fall along predicted meltwater mixing lines in θ-S space (Figure 2b) and therefore appear to be the result of submarine meltwater that was in direct contact with ambient fjord waters—that is, a product of ambient melting. There is no detectable modification from subglacial discharge in these intrusions, so we attribute them to ambient melting and not discharge-driven melting. (We do, however, see a strong signal of subglacial discharge in the upper 30 m where the discharge plume is flowing away from the glacier, Figures 1d, 1e, and 2, and supporting information.) The large temperature anomalies in the intrusions are salinity compensated, such that the density profile is stably stratified (Figure 2a), so these cold layers appear to be anomalous features of glacier origin and associated with lateral transport. Given these characteristics, we posit that the cold layers are the signal of ambient melt intrusions—a mixture of submarine melt and fjord waters—after the upwelling ambient plumes have reached their neutral buoyancy and started intruding horizontally into the fjord. Thus, we refer to these cold layers as meltwater intrusions.

We identify 95 intrusions that meet two criteria: (i) a cold anomaly of at least −0.2 °C over a vertical thickness of >4 m, and also (ii) a peak anomaly of at least −0.5 °C (anomalies calculated on isopycnals, relative to

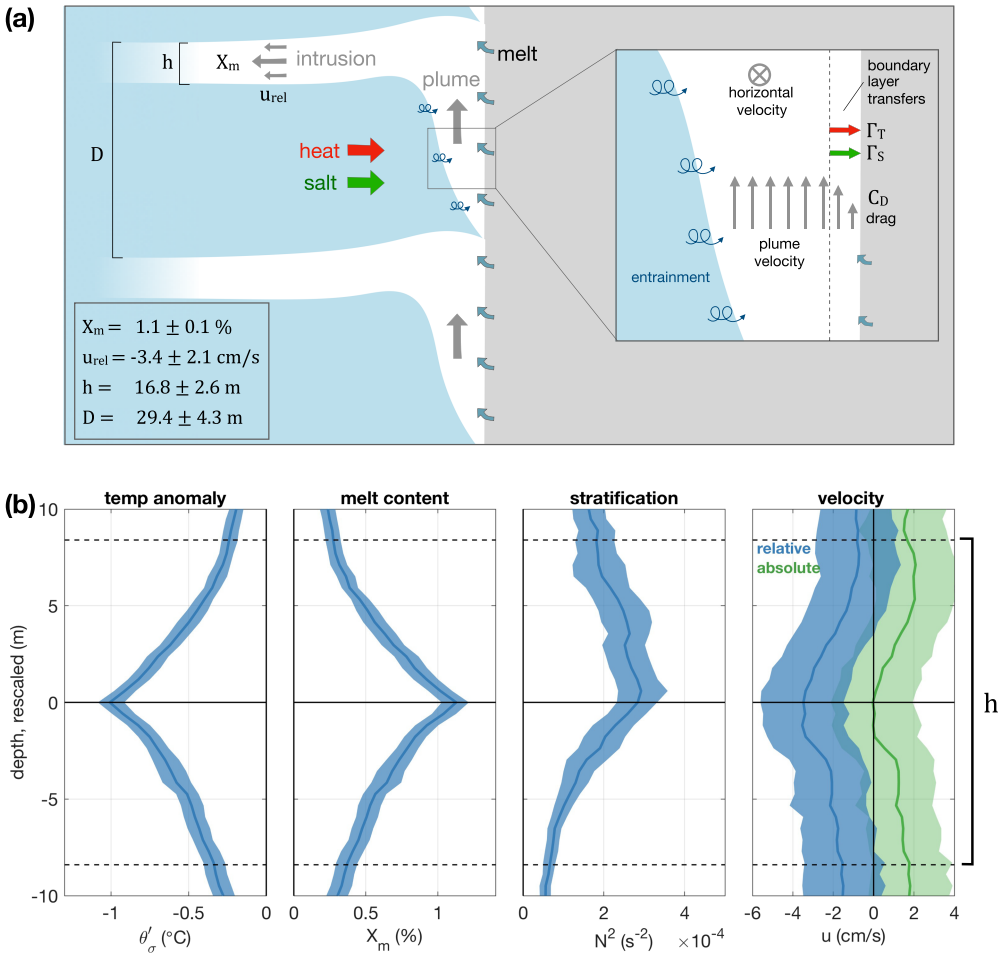

Figure 3. Typical characteristics of ambient melt intrusions. (a) Schematic of ambient melt plume and intrusion, with an inset showing additional details of the upwelling plume. Variables are shown schematically, and results in lower left box are from composite of observations. (b) Composite of 95 intrusions, selected with criteria of $\theta'_\sigma < -0.5$ °C and vertical thickness of >4 m. From left to right: isopycnal temperature anomaly, melt content, stratification, and eastward velocity. Velocity is shown both as absolute velocity (green) and relative velocity (anomaly relative to mean near-glacier velocity). Error bars are bootstrap 95% confidence intervals. Before averaging, the depth dimension, z, of each intrusion is rescaled as $z_{rescale} = (z - z_{\theta' \max})\frac{\langle h \rangle}{h}$ where $z_{\theta' \max}$ is the depth of the maximum temperature anomaly, h is the thickness of the intrusion, and $\langle h \rangle$ is the average thickness of all intrusions.

downstream fjord properties). For each intrusion, we quantify the meltwater content by assuming that (a) the ambient fjord waters that have been entrained are linear in θ-S space in the vicinity of the intrusion, and (b) there is no contribution from subglacial discharge, which has its own unique θ-S characteristics. This allows us to derive not only the meltwater content (Figure 2a) but also the average θ-S properties of entrained fjord waters, the mean depth of the entrained waters for each intrusion, and the vertical scale of upwelling for ambient melt plumes (supporting information).

We average the properties of all 95 intrusions to create a composite that describes the typical characteristics of the meltwater intrusions (Figure 3). On average, the intrusions have a maximum meltwater content (X_m) of 1.1 ± 0.1%, an isopycnal temperature anomaly (θ'_σ) of −1.0±0.1 °C, and a velocity (u_{rel}) of 3.4 ± 2.1 cm/s away from the glacier, relative to the mean velocity (all quoted with bootstrap 95% confidence limits). The intrusions are also characterized by a peak in stratification—they are most frequently observed near the pycnocline and are also associated with a positive anomaly in stratification relative to the mean. The average vertical rise of the plumes, D, is 29.4 ± 4.3 m, and the average thickness of the intrusions, h, is 16.8 ± 2.6 m.

There is no signal of meltwater intrusions beyond 400 m from the glacier (Figure 1c and supporting information), which we attribute to the subglacial discharge-driven circulation. The meltwater intrusions

Table 1
Comparing Observations With Plume-Melt Theory

Observations or theory	Parameter adjustments	Melt content X_m (%)	Vertical rise D (m)	Melt rate $\overline{m}$ (m/day)
Observed intrusions		1.1 ± 0.1	29 ± 4	6.1[1.7 14.4][a]
Observed fjord budgets				5.5 ± 1.0[b]
Theory: standard values of $C_D, \Gamma_{S,T}, v_{hor} = 0$		0.09	3.1	0.05
Theory: one parameter adjusted	$v_{hor} = 0.85$ m/s	1.1	27	6.0
to match observations	$C_D \times 175$	1.1	33	3.0
	$\Gamma_{S,T} \times 13$	1.1	36	6.5
Theory: realistic velocity	$C_D \times 14$	1.1	28	5.4
of v_{hor}=0.2 m/s with other	$\Gamma_{S,T} \times 4$	1.1	27	5.7
parameters adjusted	$C_D \times 4, \Gamma_{S,T} \times 2$	1.1	27	5.7
to match observations				

Note. The first row has average properties of observed melt intrusions, while the second row shows the melt estimate based on the fjord budgets. Results from plume-melt theory (i.e., predictions for the terminal properties of upwelling ambient plumes) are shown for both the standard coefficient values and with parameters adjusted to match the observed meltwater fraction of 1.1%. Standard values for the drag coefficient (C_D) and the thermal and saline transfer coefficients (Γ_T, Γ_S) are as follows: $C_D = 2.5 \times 10^{-3}$, $\Gamma_T = 2.2 \times 10^{-2}$, $\Gamma_S = 6.2 \times 10^{-4}$.
[a]The melt rate from the observed intrusions is shown in gray because it is derived from an approximate scaling. [b]The melt rate inferred from fjord budgets should correspond to a terminus-average melt rate, while all the other melt rates are estimates of the ambient melt rate in particular (excluding any discharge-driven melting).

are primarily observed below 30 m where the flow is, on average, moving toward the glacier at 2 to 5 cm/s (Figures 1d and 1e). The intrusions, on the other hand, are moving away from the glacier at 3.4 ± 2.1 cm/s relative to this mean velocity and are approximately stagnant (0.1 ± 2.0 cm/s) in their absolute velocity (Figure 3b). Thus, the intrusions are fighting against the larger-scale circulation and appear to be eventually entrained into the subglacial discharge plume along with the inflowing fjord waters. This could explain the absence of intrusions beyond 400 m and suggests that the intrusions' meltwater (the product of ambient melting) is ultimately exported with the subglacial discharge plume near the surface.

4. Discrepancy Between Observations and Standard Plume-Melt Theory

The observed signal of melt intrusions is significantly larger than standard theory predicts for ambient melting (Figure 2b). Using the plume-melt framework of coupling buoyant plume theory to a melt parameterization with typical coefficient values (e.g., Cowton et al., 2015; Jenkins, 2011; Magorrian & Wells, 2016), ambient melt plumes are predicted to have a vertical rise (D) of 3 m, form intrusions with 0.09% meltwater content, and drive 0.05 m/day of melting (Table 1 and supporting information). However, the observed intrusions have an average vertical rise of 29 ± 4 m and meltwater content of 1.1 ± 0.1%—both an order of magnitude larger than standard theory. The ratio of melt to entrainment must be significantly higher than theory predicts in order to produce the observed meltwater intrusions.

Given this discrepancy, we examine how the coupled plume-melt parameterization could be adjusted to align with the observations. The theory relies critically on turbulent transfer coefficients for heat and salt (Γ_T, Γ_S) and a drag coefficient (C_D), and a standard set of values has been used in almost all studies of tidewater glaciers (e.g., Carroll et al., 2016; Cowton et al., 2015; Jenkins, 2011; Magorrian & Wells, 2016; Sciascia et al., 2013; Slater et al., 2016, and many others). However, these coefficients are empirically derived from horizontal ice interfaces (sea ice and ice shelves; e.g., Jenkins et al., 2010; McPhee et al., 1987) and have not been validated for near-vertical termini. There are several ways one could adjust these coefficients to yield the observed meltwater content (Table 1). For example, in order to create intrusions with meltwater content of 1.1% by adjusting the drag coefficient, C_D would have to increase from the standard value of 2.5×10^{-3} to 0.4, that is, by a factor of 175. Alternatively, to match the observations by adjusting the turbulent transfer coefficients, Γ_T and Γ_S would both have to increase by a factor of 13.

We also explore a new modification to buoyant plume theory by adding the effect of an external, horizontal velocity. While previous studies have examined the impact of horizontal velocities—modeled or

observed—using the melt parameterization alone (e.g., Cai et al., 2017; Slater et al., 2018), here we retain the plume component and modify the coupled plume-melt theory to include a prescribed horizontal velocity (supporting information). The horizontal velocity directly increases the melt rate and indirectly increases the vertical rise of the plume by increasing the buoyancy forcing. This modification to plume-melt theory allows us to explore the impact of the horizontal velocity not only on the melt rate—as in previous studies—but also on the meltwater products (plume and intrusion) from ambient melting.

If the coefficients (Γ_T, Γ_S, and C_D) are kept at their standard values, a mean horizontal velocity of 0.85 m/s along the ice face is required to match the observations. Alternatively, the observed intrusions can be matched by using the observed along-ice horizontal velocity of 0.2 m/s (Figure S7 in the supporting information) and also increasing the drag and turbulent transfer coefficients by more modest factors of 4 and 2, respectively (Table 1).

We cannot say which, if any, of these scenarios is correct—most likely the inclusion of the horizontal velocity field and modifications to the empirical coefficients are both needed. But, importantly, in all of these scenarios where we adjust theory to match the observations, the resulting melt rates are 3–6 m/day (Table 1), which is 2 orders of magnitude greater than the standard theoretical estimate of 0.05 m/day. Thus, if the basic physics of plume-melt theory is correct (a shear-driven boundary layer and entrainment proportional to velocity; supporting information), then our observations suggest that (1) critical parameters in the plume-melt parameterization must be adjusted, and (2) ambient melt rates are 100 times higher than expected.

5. Corroborating Evidence for Elevated Ambient Melting

In addition to the comparison between observed intrusions and plume-melt theory, there are three other pieces of evidence that point toward elevated ambient melt rates of ~5 m/day:

(a) *Fjord Budgets to Infer Meltwater Flux*. Using 10 cross-fjord transects of velocity and water properties, we evaluate budgets of heat, salt, and mass (Jackson & Straneo, 2016; Motyka et al., 2003; Sutherland et al., 2019) to estimate the flux of submarine meltwater and subglacial discharge through the fjord (supporting information). The average meltwater flux is 9.8 ± 1.7 m^3/s, which corresponds to a terminus-averaged melt rate of 5.5 ± 1.0 m/day. The standard plume-melt parameterization would give a maximum terminus-averaged melt rate of only 1.1 ± 0.1 m/day, based on combining discharge-driven melting of 8.0 ± 0.8 m/day over 13% of the terminus and 0.05 m/day of ambient melting over the other 87% (supporting information). Thus, the fluxes inferred from fjord budgets also indicate that melt rates are significantly higher than standard theory predicts.

(b) *Scaling for Melt Rate From Intrusions*. With the observed intrusions' properties and relative velocity, we can estimate the magnitude of ambient melting using a simple scaling that does not rely on plume-melt theory. Neglecting the cross-terminus dimension, a steady-state equation for the conservation of meltwater is

$$\int_{z_0}^{z_0+h} u_{rel} X_m \mathrm{d}z = \bar{m} D \tag{1}$$

where the meltwater exported by an intrusion over its thickness, h (left-side integral) must equal the input from melting (right-side, depth-average melt multiplied by the vertical rise of the plume). Using our observations to estimate D and the left-side integral, we estimate a mean melt rate of $\bar{m} = 6.1$ [1.7 14.4] m/day (with bootstrap 95% confidence interval) over the vertical rise of the ambient plumes (supporting information). While there is significant uncertainty in this estimate, even the lower bound of 1.7 m/day is more than an order of magnitude larger than standard theory would predict for ambient melting.

(c) *Acoustic Detection of Terminus Ice Loss*. The inferred ambient melt rates also align with independent measurements of LeConte Glacier from multibeam sonar surveys (Sutherland et al., 2019). By differencing repeat multibeam scans, the terminus-averaged melt rates are estimated to be 5.2 m/day in August 2016 and 1.3 m/day in May 2017 (compared to standard plume melt estimates of 0.9 ± 0.4 and 0.5 ± 0.3 m/day for these time periods, respectively). Our results corroborate the findings of Sutherland et al. (2019)—that submarine melt rates are significantly higher than theory predicts—and the intrusions described here reveal the importance of ambient melting for explaining the elevated melt rates.

6. Implications for Net Terminus Ablation and Ocean-Glacier Interactions

We have found a strong signal of ambient melting in the vicinity of an energetic subglacial discharge plume, and our results suggest that ambient melt is a significant—and previously neglected—component of the net ablation (calving plus melting) at the terminus. During the surveying period, ambient melting of ~5 m/day should balance ~33% of the incoming ice flux locally over ambient melt regions of the terminus, based on a mean ice velocity of 15 m/day. The maximum ice velocity (18 m/day) also provides an upper limit on the discharge-driven melt rate, given that the terminus position was relatively stable. Using this upper limit, ambient melting should constitute at least ~65% of the total melt budget (compared to 4% predicted by standard plume-melt theory). Additionally, the total melt over the entire terminus should balance at least one third of the incoming ice flux (similar to the conclusions of Motyka et al., 2013), whereas standard theory would predict that total melt balances only 7% of the ice flux. Thus, our results indicate that modeling of terminus ablation and glacier dynamics requires accurate representation of ambient melting.

We show that ambient melt intrusions are only observable by autonomous sampling within 400 m of LeConte's terminus. Measurements made further downstream (which are the only observations available at most tidewater glaciers) show no signal of these meltwater intrusions—instead, the meltwater is ultimately exported near the surface after mixing with the subglacial discharge plume. This is consistent with observed patterns of glacially modified waters in other fjords, where the downstream distribution of submarine meltwater is highly correlated with subglacial discharge (e.g., Beaird et al., 2017, 2018). Thus, submarine meltwater—at LeConte and in other fjords—might often look like discharge-driven melting, despite being the product of ambient melting (as also hypothesized by Mankoff et al., 2016).

While our observations are limited to one glacier-fjord system, corroborating evidence of ambient meltwater intrusions can be found in the near-glacier observations of Everett et al. (2018) and Mankoff et al. (2016), which show similar cold layers with properties along the meltwater mixing line. However, these and other studies using near-glacier observations (Bendtsen et al., 2015; Everett et al., 2018; Jackson et al., 2017; Mankoff et al., 2016) have focused on subglacial discharge plume dynamics without any characterization of ambient melt processes.

We hypothesize that the ambient melt dynamics described here should be similar at Greenlandic glaciers, although the signal of intrusions might be less discernible because the θ-S properties of coastal waters around Greenland often coincide with the meltwater mixing line (Straneo et al., 2012). For example, using the ocean conditions near Helheim Glacier, Greenland (Beaird et al., 2018), plume-melt theory with standard coefficients would predict an average ambient melt rate of 0.12 m/day. With the smallest theoretical adjustments that match LeConte observations ($C_d \times 4$, $\Gamma \times 2$ and $v_{hor} = 0.2$ m/s; last line of Table 1), the ambient melt rate for Helheim would jump to 3.2 m/day and become a significant component of Helheim's total ice discharge (~20 m/day, Bevan et al., 2015).

In the various attempts to match theory with our observations (Table 1), there is a physical basis for the direction of each adjustment. The standard transfer coefficients have only been tested at near-horizontal ice faces (Jenkins et al., 2010; McPhee et al., 1987)—where meltwater enhances stratification—and likely underestimate the turbulent transfer at near-vertical termini, where meltwater input is convectively unstable (Straneo & Cenedese, 2015). Additionally, the standard drag coefficient assumes a planar ice surface and could underestimate the roughness of the terminus (Gwyther et al., 2015).

The scenarios that include a horizontal velocity are considered the most plausible—both because an energetic velocity field is observed and because its inclusion in plume-melt theory reduces the difference between ambient and discharge-driven melt rates. Recent evidence suggests that melt rates should not differ as drastically across the terminus as standard theory predicts (Sutherland et al., 2019; Wagner et al., 2019). The scenarios where only $\Gamma_{T,S}$ or C_D are adjusted (Table 1) seem least plausible because they would create unrealistically large discharge-driven melting if the coefficients are uniform across the terminus. For example, if $\Gamma_{T,S}$ increased by a factor of 13, discharge-driven melt would increase from 8.0 ± 0.8 to 96 ± 10 m/day, which is significantly higher than the ice flux into the terminus (18 m/day). Even the scenario including a realistic horizontal velocity with smaller coefficient adjustments ($C_D \times 4$ and $\Gamma_{T,S} \times 2$) would result in discharge-driven melting of 30 ± 3 m/day, which is still larger than the ice velocity (though approaching a similar magnitude). Therefore, a simple adjustment of the coefficients might not lead to a generalizable melt parameterization for both regimes of melt, unless there is a physical basis for varying the coefficients

across the terminus. For example, C_D could have a different value behind the discharge plume, both due to differences in ice roughness and because C_D might depend on the Reynolds number of the flow (Ezhova et al., 2018).

Further evidence for the importance of the horizontal velocity field is found in the sonar-derived melt rates from Sutherland et al. (2019). Terminus-averaged melt rates were observed to be 4 times higher in August than in May, whereas standard plume-melt theory predicts that ambient melt rates should be slightly higher in May. Enhanced melting in August could be attributed to a more energetic velocity field, since speeds near the terminus (derived from iceberg tracking) were 2–3 times higher in August than in May (Sutherland et al., 2019). Ultimately, if the horizontal velocity from a discharge-driven recirculation (e.g., Kienholz et al., 2019; Slater et al., 2018) plays a critical role in enhancing ambient melting, then ambient melt rates will be linked to discharge—even though ambient melting is not directly driven by the discharge plume. However, other processes (tides, winds, internal waves, etc.) could drive along-ice velocities and decouple ambient melting from subglacial discharge.

Additional observations of the ocean-ice boundary layer are needed to validate the underlying functional form of the melt parameterization. The standard melt parameterization (Holland & Jenkins, 1999, etc.) assumes a shear-driven boundary layer, but recent laboratory and direct numerical simulation studies (e.g., Kerr & McConnochie, 2015; McConnochie & Kerr, 2017; Mondal et al., 2019) find that boundary-layer fluxes can be driven by convective instabilities, such that the melt rate becomes independent of plume velocity. While this latter regime is unlikely at a relatively warm, energetic system like LeConte (McConnochie & Kerr, 2017), the variety of existing theories highlights a need for testing the functional form of our melt parameterizations, not just the empirical coefficients therein.

7. Conclusions

We have shown that meltwater intrusions are ubiquitous near LeConte Glacier, and, even in the vicinity of an energetic subglacial discharge plume, there is a strong signal of ambient melting. Our observations indicate that ambient melting is 100 times higher than expected using existing theory (~5 m/day, instead of 0.05 m/day) and an important—but previously neglected—part of the total melt budget. Several different pieces of evidence point toward this conclusion: (1) a comparison between observed intrusions and plume-melt parameterizations; (2) a melt conservation scaling from the observed intrusions; and (3) meltwater fluxes derived from downstream fjord measurements of heat and salt transport. Our conclusions of elevated ambient melting are further corroborated by independent estimates of melting from multibeam sonar (Sutherland et al., 2019). The discrepancy between observations and existing plume-melt parameterizations is likely due to a combination of the horizontal velocity field and the use of empirical coefficients that are untested at tidewater glaciers. Additional observations of the ocean-ice boundary layer are needed to create a generalizable melt parameterization for modeling ocean-glacier interactions and sea level rise.

Acknowledgments
This work was funded by NSF OPP Grants 1503910, 1504191, 1504288, and 1504521 and National Geographic Grant CP4-171R-17. Additionally, this research was supported by the NOAA Climate and Global Change Postdoctoral Fellowship Program, administered by UCAR's Cooperative Programs for the Advancement of Earth System Science (CPAESS) under award #NA18NWS4620043B. These observations would not be possible without the skilled engineering team who developed the autonomous kayaks—including Jasmine Nahorniak, June Marion, Nick McComb, Anthony Grana, and Corwin Perren—and also the Captain and crew of the M/V *Amber Anne*. We thank Donald Slater and an anonymous reviewer for valuable feedback that improved this manuscript. *Data availability:* All of the oceanographic data collected by ship and kayak have been archived with the National Centers for Environmental Information (Accession 0189574, https://accession.nodc.noaa.gov/0189574). The glacier data have been archived at the Arctic Data Center (https://doi.org/10.18739/A22G44).

References

Alley, R. B., Anandakrishnan, S., Christianson, K., Horgan, H. J., Muto, A., Parizek, B. R., et al. (2015). Oceanic forcing of ice-sheet retreat: West Antarctica and more. *Annual Review of Earth and Planetary Sciences*, *43*(1), 207–231.

Bamber, J. L., Tedstone, A. J., King, M. D., Howat, I. M., Enderlin, E. M., van den Broeke, M. R., & Noel, B. (2018). Land ice freshwater budget of the Arctic and North Atlantic Oceans: 1. Data, methods, and results. *Journal of Geophysical Research: Oceans*, *123*, 1827–1837. https://doi.org/10.1002/2017JC013605

Beaird, N., Straneo, F., & Jenkins, W. (2017). Characteristics of meltwater export from Jakobshavn Isbræ and Ilulissat Icefjord. *Annals of Glaciology*, *58*(74), 107–117.

Beaird, N. L., Straneo, F., & Jenkins, W. (2018). Export of strongly diluted Greenland meltwater from a major glacial fjord. *Geophysical Research Letters*, *45*, 4163–4170. https://doi.org/10.1029/2018GL077000

Bendtsen, J., Mortensen, J., Lennert, K., & Rysgaard, S. (2015). Heat sources for glacial ice melt in a west Greenland tidewater outlet glacier fjord: The role of subglacial freshwater discharge. *Geophysical Research Letters*, *42*, 4089–4095. https://doi.org/10.1002/2015GL063846

Bevan, S. L., Luckman, A., Khan, S. A., & Murray, T. (2015). Seasonal dynamic thinning at Helheim Glacier. *Earth and Planetary Science Letters*, *415*(C), 47–53.

Cai, C., Rignot, E., Menemenlis, D., & Nakayama, Y. (2017). Observations and modeling of ocean-induced melt beneath Petermann Glacier Ice Shelf in northwestern Greenland. *Geophysical Research Letters*, *44*, 8396–8403. https://doi.org/10.1002/2017GL073711

Carroll, D., Sutherland, D. A., & Hudson, B. (2016). The impact of glacier geometry on meltwater plume structure and submarine melt in Greenland fjords. *Geophysical Research Letters*, *43*, 9739–9748. https://doi.org/10.1002/2016GL070170

Cowton, T., Slater, D., Sole, A., Goldberg, D., & Nienow, P. (2015). Modeling the impact of glacial runoff on fjord circulation and submarine melt rate using a new subgrid-scale parameterization for glacial plumes. *Journal of Geophysical Research: Oceans*, *120*, 796–812. https://doi.org/10.1002/2014JC010324

Dieng, HB, Cazenave, A., Meyssignac, B., & Ablain, M. (2017). New estimate of the current rate of sea level rise from a sea level budget approach. *Geophysical Research Letters, 44*, 3744–3751. https://doi.org/10.1002/2017GL073308

Ellison, T. H., & Turner, J. S. (1959). Turbulent entrainment in stratified flows. *Journal of Fluid Mechanics*, *6*, 423–448.
Everett, A., Kohler, J., Sundfjord, A., Kovacs, K., Torsvik, T., Pramanik, A., et al. (2018). Subglacial discharge plume behaviour revealed by CTD-instrumented ringed seals. *Scientific Reports*, *8*, 13467.
Ezhova, E., Cenedese, & Brandt, L. (2018). Dynamics of three-dimensional turbulent wall plumes and implications for estimates of submarine glacier melting. *Journal of Physical Oceanography*, *48*(9), 1941–1950.
Fried, M. J., Catania, G. A., & Bartholomaus, T. C. (2015). Distributed subglacial discharge drives significant submarine melt at a Greenland tidewater glacier. *Geophysical Research Letters*, *42*, 9328–9336. https://doi.org/10.1002/2015GL065806
Gade, H. G. (1979). Melting of ice in sea water: A primitive model with application to the Antarctic ice shelf and icebergs. *Journal of Physical Oceangraphy*, *9*(1), 189–198.
Gwyther, D. E., Galton-Fenzi, B. K., Dinniman, M. S., Roberts, J. L., & Hunter, J. R. (2015). The effect of basal friction on melting and freezing in ice shelf-ocean models. *Ocean Modelling*, *95*(C), 38–52.
Holland, & Jenkins, A. (1999). Modeling thermodynamic ice-ocean interactions at the base of an ice shelf. *Journal of Physical Oceangraphy*, *29*(8), 1787–1800.
Holland, D. M., Thomas, R. H., de Young, B., Ribergaard, M. H., & Lyberth, B. (2008). Acceleration of Jakobshavn Isbrætriggered by warm subsurface ocean waters. *Nature Geoscience*, *1*(10), 659–664.
Huppert, H. E., & Turner, J. S. (1980). Ice blocks melting into a salinity gradient. *Journal of Fluid Mechanics*, *100*, 367–384.
Jackson, R. H., Shroyer, E. L., Nash, J. D., Sutherland, D. A., Carroll, D., Fried, M. J., et al. (2017). Near-glacier surveying of a subglacial discharge plume: Implications for plume parameterizations. *Geophysical Research Letters*, *39*, 6886–6894. https://doi.org/10.1002/2017GL073602
Jackson, R. H., & Straneo, F. (2016). Heat, salt, and freshwater budgets for a glacial fjord in Greenland. *Journal of Physical Oceanography*, *46*(9), 2735–2768.
Jenkins, A. (2011). Convection-driven melting near the grounding lines of ice shelves and tidewater glaciers. *Journal of Physical Oceanography*, *41*(12), 2279–2294.
Jenkins, A., Nicholls, K. W., & Corr, HughF. J. (2010). Observation and parameterization of ablation at the base of Ronne Ice Shelf, Antarctica. *Journal of Physical Oceanography*, *40*(10), 2298–2312.
Kerr, R. C., & McConnochie, C. D. (2015). Dissolution of a vertical solid surface by turbulent compositional convection. *Journal of Fluid Mechanics*, *765*, 211–228.
Kienholz, C., Amundson, J. M., Motyka, R. J., Jackson, R. H., Mickett, J. B., Sutherland, D. A., et al. (2019). Tracking icebergs with time-lapse photography and sparse optical flow, LeConte Bay, Alaska, 2016-2017. *Journal of Glaciology*, *11*, 1–17.
Luckman, A., Benn, D. I., Cottier, F., Bevan, S., Nilsen, F., & Inall, M. (2015). Calving rates at tidewater glaciers vary strongly with ocean temperature. *Nature Communications*, *6*, 1–7.
Ma, Y., & Bassis, J. N. (2019). The effect of submarine melting on calving from marine terminating glaciers. *Journal of Geophysical Research: Earth Surface*, *3*, 334–346. https://doi.org/10.1029/2018JF004820
MacAyeal, D. R. (1985). Evolution of tidally triggered meltwater plumes below ice shelves. *Oceanology of the Antarctic continental shelf* (pp. 133–143). Washington, DC: AGU.
Magorrian, S. J., & Wells, A. J. (2016). Turbulent plumes from a glacier terminus melting in a stratified ocean. *Journal of Geophysical Research: Oceans*, *121*, 4670–4696. https://doi.org/10.1002/2015JC011160
Mankoff, K. D., Straneo, F., Cenedese, Das, S. B., Richards, C. G., & Singh, H. (2016). Structure and dynamics of a subglacial discharge plume in a Greenlandic fjord. *Journal of Geophysical Research: Oceans*, *121*, 8670–8688. https://doi.org/10.1002/2016JC011764
McConnochie, C. D., & Kerr, R. C. (2017). Testing a common ice-ocean parameterization with laboratory experiments. *Journal of Geophysical Research: Oceans*, *122*, 5905–5915. https://doi.org/10.1002/2017JC012918
McPhee, M. G., Maykut, G. A., & Morison, J. H. (1987). Dynamics and thermodynamics of the ice/upper ocean system in the marginal ice zone of the Greenland Sea. *Journal of Geophysical Research*, *92*(C7), 7017–7031.
Mondal, M., Gayen, B., Griffiths, R. W., & Kerr, R. C. (2019). Ablation of sloping ice faces into polar seawater. *Journal of Fluid Mechanics*, *863*, 545–571.
Morton, B. R., Taylor, G., & Turner, J. S. (1956). Turbulent gravitational convection from maintained and instantaneous sources. *Proceedings of the Royal Society of London A: Mathematical, Physical and Engineering Sciences*, *234*(1196), 1–23.
Motyka, R. J., Dryer, W. P., Amundson, J., Truffer, M., & Fahnestock, M. (2013). Rapid submarine melting driven by subglacial discharge, LeConte Glacier, Alaska. *Geophysical Research Letters*, *40*, 5153–5158. https://doi.org/10.1002/grl.51011
Motyka, R. J., Hunter, L., Echelmeyer, K. A., & Connor, C. (2003). Submarine melting at the terminus of a temperate tidewater glacier, LeConte Glacier, Alaska, USA. *Annals of Glaciology*, *36*, 57–65.
Nash, J., Marion, J., McComb, N., Nahorniak, J., Jackson, R. H., Perren, C., et al. (2017). Autonomous CTD profiling from the Robotic Oceanographic Surface Sampler. *Oceanography*, *30*(2), 110–112.
Nick, F. M., Vieli, A., Howat, I. M., & Joughin, I. (2009). Large-scale changes in Greenland outlet glacier dynamics triggered at the terminus. *Nature Geoscience*, *2*(2), 110–114.
Sciascia, R., Straneo, F., Cenedese, C., & Heimbach, P. (2013). Seasonal variability of submarine melt rate and circulation in an East Greenland fjord. *Journal of Geophysical Research: Oceans*, *118*, 2492–2506. https://doi.org/10.1002/jgrc.20142
Shepherd, A., IMBIE, & team (2018). Mass balance of the Antarctic Ice Sheet from 1992 to 2017. *Nature*, *558*(7709), 219–222.
Slater, D., Goldberg, D. N., Nienow, P. W., & Cowton, T. R. (2016). Scalings for submarine melting at tidewater glaciers from buoyant plume theory. *Journal of Physical Oceanography*, *46*, 1839–1855.
Slater, D., Nienow, P. W., & Cowton, T. R. (2015). Effect of near-terminus subglacial hydrology on tidewater glacier submarine melt rates. *Geophysical Research Letters*, *42*, 2861–2868. https://doi.org/10.1002/2014GL062494
Slater, D., Straneo, F., Das, S. B., Richards, C. G., Wagner, T. J. W., & Nienow, P. W. (2018). Localized plumes drive front-wide ocean melting of a Greenlandic tidewater glacier. *Geophysical Research Letters*, *45*, 12,350–12,358. https://doi.org/10.1029/2018GL080763
Straneo, & Cenedese (2015). The dynamics of Greenland's glacial fjords and their role in climate. *Annual Review of Marine Science*, *7*(1), 89–112.
Straneo, F., & Heimbach (2013). North Atlantic warming and the retreat of Greenland's outlet glaciers. *Nature*, *504*(7478), 36–43.
Straneo, F., Sutherland, D. A., Holland, D., Gladish, C., Hamilton, G. S., Johnson, H. L., et al. (2012). Characteristics of ocean waters reaching Greenland's glaciers. *Annals of Glaciology*, *53*(60), 202–210.
Sutherland, D. A., Jackson, R. H., Kienholz, C., Amundson, J. M., Dryer, W. P., Duncan, D., et al. (2019). Direct observations of submarine melt and subsurface geometry at a tidewater glacier. *Science*, *365*, 3690–3374.
Wagner, T. J. W., Straneo, F., Richards, C. G., Slater, D. A., Stevens, L. A., Das, S. B., & Singh, H. (2019). Large spatial variations in the flux balance along the front of a Greenland tidewater glacier. *The Cryosphere*, *13*(3), 911–925.